Sensors & Actuators: A. Physical 379 (2024) 115996

Contents lists available at ScienceDirect

Sensors and Actuators: A. Physical

journal homepage: www.journals.elsevier.com/sensors-and-actuators-a-physical

The effects of Ppy-silicene composite on the performance of n-/p-type silicon semiconductor-based photodiodes

Abdulkerim Karabulut [a,*], D.E. Yıldız [b,*], M. Yıldırım [c], H.H. Güllü [d], A. Kocyigit [e], N. Tasaltın [f,g,h,i], A. Gulsaran [j], B. Bastug Azer [j], M. Yavuz [j,k]

[a] Department of Basic Sciences, Faculty of Sciences, Erzurum Technical University, Erzurum, Turkey
[b] Department of Physics, Hitit University, Çorum 19030, Turkey
[c] Department of Biotechnology, Faculty of Science, Selcuk University, Konya 42030, Turkey
[d] Microelectronics, Guidance and Electro-Optics Division, Optical and Optomechanical Design Department, ASELSAN Inc., Ankara 06200, Turkey
[e] Department of Electronics and Automation, Vocational High School, Bilecik Şeyh Edebali University, Bilecik 11000, Turkey
[f] Environment and Energy Technologies Research Center, Maltepe University, Istanbul 34840, Turkey
[g] Department of Basic Sciences, Maltepe University, Istanbul 34840, Turkey
[h] Dept. of Renewable Energy Tech. and Management, Maltepe University, Istanbul 34840, Turkey
[i] CONSENS Inc., Maltepe University Research Center, Technopark Istanbul, Istanbul 34840, Turkey
[j] Waterloo Institute for Nanotechnology (WIN), University of Waterloo, ON, Canada
[k] Mechanical and Mechatronic Engineering Department, University of Waterloo, ON, Canada

ARTICLE INFO

Keywords:
Polypyrrole (PPy)
Silicene
Photodiode
Protoresponse
Composites

ABSTRACT

The advancement of electronic technology is accelerated by the discovery of two-dimensional materials, and it also becomes a prompting area for researchers to focus on exploring their alternatives. In these research activities, silicene attracts significant attention due to its potential in various electronic applications. In addition, polypyrrole (PPy), belonging to the class of intrinsic conducting polymers, is another important material preferentially used in this technology. In this study, a composite material prepared in the form of Ppy:silicene is applied between metal and semiconductor. The resulting Ppy:silicene/p-Si and Ppy:silicene/n-Si photodiodes are discussed according to their diode responses. Structural characteristics of fabricated silicene based layer material are determined by X-ray diffraction technique. Device behaviors of the fabricated devices are mainly analyzed in response to incident light. At this characterization step, electrical measurements are conducted in a dark environment and under different light intensities ranging from 20 to 100 mW/cm^2. For instance, the Ppy-Silicene/p-Si device exhibited a barrier height of 0.57 eV and an ideality factor of 3.1, compared to the Ppy-Silicene/n-Si device, which showed a barrier height of 0.55 eV and an ideality factor of 4.9. Characteristic photodiode parameters, such as light sensitivity, responsivity, and detectivity are obtained through current-voltage/time measurements depending on power of light. In addition to these parameters, performance-determining parameters for the diodes as barrier height, series resistance, and ideality factor are investigated according to thermionic emission and Cheung's approaches. The results indicate that the performance of the Ppy-Silicene/p-Si photodiode is significantly more effective than that of the photodiode produced with n-Si substrate. As a result of these experimental works, the fabricated Ppy-Silicene composite material and its diodes, especially on p-Si, can be evaluated as a promising candidate for optoelectronic technology.

1. Introduction

In electronic technology, optoelectronics is a significant branch that combines aspects of both optics and electronics. It is important to highlight that these devices have various applications in fields such as automatic control systems, medicine, the military, and telecommunications [1–4]. Basically, optoelectronic mechanisms work to generate electrical energy in response to the incident light. It means that electric current is obtained by photoelectric transducers when exposed to light [5,6]. The photo-response can be found in a system made of multiple p-n

* Corresponding authors.
E-mail addresses: akerimkara@gmail.com (A. Karabulut), desrayildiz@hitit.edu.tr (D.E. Yıldız).

https://doi.org/10.1016/j.sna.2024.115996
Received 2 September 2024; Received in revised form 13 October 2024; Accepted 20 October 2024
Available online 21 October 2024

junctions interconnected in series. Among these p-n junctions, one junction is exceptionally thin, allowing easy passage of light. Thus, the process is mainly due to absorption of light energy by a semiconductor material at junction region. This light absorption can form charge carriers as a result of electron excitation and causing holes in their states [7–9]. Photo-generated electron-hole pairs result in a voltage generation. Each photovoltaic junction typically produces a voltage of around 0.6 V. To generate higher voltages, extensive arrays of solar cells can be interconnected in both series and parallel configurations [10,11]. Therefore, photovoltaic devices can offer a useful option to supply electricity as an alternative way to the conventional power sources [12]. In addition, they can be found in space applications to charge solar batteries [10,11].

As another device application under illumination, photodiodes inherently have high electrical impedance and usually operated with an applied reverse voltage. Reverse biasing results in increasing depletion width that reduces the capacitance of the diode and improves its response time and sensitivity to light. Serving as high-speed sensors, they produce a small current (measured in microamperes) directly proportional to the light intensity [13,14]. Photons possess enough energy to break several covalent bonds within the junction and so that generates electron-hole pairs and consequently flow of current within the diode. An increase of light intensity prompts photodiode to release additional charge carrier pairs and as a result amplifying the generated current [15–17]. At these applications, the structure can be fabricated by organic materials in addition to conventional inorganic counterparts. Basically, organic solar cells (OSCs) and organic photodetectors (OPDs) have similar device configurations whereas their functions are different. OSCs are mainly designed to produce electricity efficiently under illumination. On the other hand, OPDs are optimized for detecting light with high sensitivity and responding to variations in light intensity. The crucial parameters for these structures are dark- and photo-generated currents. These parameters are proportional to the light absorption, charge transportation, losses and extraction of free-carrier. Although there are variety of application areas, there are physical concerns about device status and mechanisms of bulk-heterojunction layers [18,19].

Researches into graphene-like two-dimensional (2D) materials are point of interest with the discovery of graphene, and these studies present various chemical compounds of transition metals [20], phosphorene [21], stanine [22], germanene [23], silicene [24], and hexagonal boron nitride [25]. Its compatibility with existing technology, as much as its remarkable optical and electrical properties, directs greater attention toward silicene compared to others [24,26]. Silicene is a 2D variation of silicon resembling graphene, however composed of silicon atoms arranged in a honeycomb lattice, holds promise as a nanomaterial due to its distinct properties [27]. Due to a 2D material, it provides large surface-to-volume ratio to increase surface interactions at interfaces. Similar to graphene, it has high electron mobility and that supports its use in electronics, especially in photovoltaic applications. In comparison to graphene, silicene exhibits lower values for the Poisson ratio, ultimate stress, bulk modulus, and Young's modulus [28]. Specifically, its in-plane stiffness constant is measured at 62 J/m^2 with a Poisson ratio of 0.3, contrasting with graphene's 335 J/m^2 and 0.16, respectively [29,30]. Moreover, bulk modulus of graphene exceeds that of silicene by a factor of 3.5 [31]. Both silicene and graphene boast unique band structures, featuring conduction and valence bands intersecting linearly at the Brillouin zone points K and K′ at the Fermi energy level. Silicene comes in two forms: buckled and flat, each exhibiting a zero π–π* gap at the K point and electronic attributes similar to graphene [32,33]. Silicene's electronic characteristics render it suitable for various applications, including photodiodes and photodetectors. The presence of a direct bandgap in specific configurations enables efficient light emission and absorption, pivotal for advancing optoelectronic devices [34]. Materials take on different characteristics through the addition or incorporation of various substances, allowing for the redesign of their electrical and optical properties. Unlike graphene, bandgap of silicine can be tuned to achieve high efficiency in optoelectronic devices.

In recent years, intrinsic conducting polymers with conjugated double bonds attracts considerable interest as advanced materials in device applications. Among them, polypyrrole (PPy) is particularly notable for commercial applications due to its superior environmental stability, straightforward synthesis, and higher conductivity compared too many other conducting polymers [35–37]. Being a conducting polymer, at device interface it can transport charges efficiently. In addition, it can be evaluated as a stable material in various applications and it presents mechanical flexibility in use for flexible and lightweight devices. It can be found in a variety of applications, such as biosensors [38], gas sensors [39], wires [40], micro-actuators [41], antiostatic coatings [42], solid electrolytic capacitors [43], electrochromic windows and displays [44], packaging [45], polymeric batteries [46], electronic devices [47], and functional membranes [48]. The material characteristics of this polymer can be tuned by doping which points way to obtain suitable charge transport layer in devices. Excellent thermal stability of PPy coatings makes them ideal for use in carbon composites. Furthermore, researchers are actively concentrated on electrochemical process parameters that affect the properties of PPy coatings [49]. This organic material can be easily synthesized through either oxidative chemical or electrochemical polymerization of pyrrole [50,51]. However, synthetic conductive material is insoluble and infusible, which limits its processing and applications in various fields. This challenge has been extensively studied, leading to the exploration of new application areas in recent years. For instance, PPy-based polymers can be used for loading and releasing drugs and biomolecules, while PPy-based polymer blends can provide corrosion protection for metals [52,53]. In fact, this composite introduces strength of the ingredients, silicene and PPy. At the interface, its component materials can facilitate charge transports where silicene acts in electron motion and PPy can conduct holes. Thus, the use of this layer at the device interface can reduce recombination loses through devices.

Various researches are documented in the literature on metal/semiconductor photodevices using various interfacial layers. However, to the best of author's knowledge, this report is a pioneer work for analysis on a silicon-based metal/semiconductor structure incorporating Ppy:Silicene as the interfacial material. Therefore, mechanisms of Ppy:Silicene/n-Si and Ppy:Silicene/p-Si are evaluated in terms of photodiode characteristics with different measurements. Besides, by using different semiconductor substrates, the importance of the material used at the interface and the semiconductor material used has also been revealed. It is expected that the outcomes of this pioneering study provide valuable discussions for future research endeavors.

2. Materials and methods

In the junction, 400 μm thick (100) crystalline oriented n-/p-type Si semiconductor wafers are used. In terms of electrical characteristics, the carrier concentration is about 7.5 × 10^{16} cm^{-3}, and the resistivity is in the range of 1–10 Ω·cm. Device fabrication is provided on 2×2 cm^2 cut the wafers. Initially, they are cleaned in an ultrasonic cleaner with dipping in acetone and isopropanol, sequentially. In order to etch natural oxide layer due to interactions of Si-O on the wafer surface, the pieces are dipped in a 1:1 HF:H_2O solution for about 30 s, and then they are rinsed and dried by nitrogen gas (N_2). Following this process, 100 nm thick Al metal layer is evaporated on one side of the wafers to build back metal contact. To enhance the ohmic behavior of this contact, p-Si/Al and n-Si/Al samples are annealed at 550 °C under N_2 environment for about 10 min. For the interface layer fabrication, PPy-silicene composite is initially obtained. The process for silicene layer involves dispersing 100 mg of Si microparticles in an equal 100 mL mixture of isopropanol and deionized water, and then sonicating them in a nitrogen-flow controlled chamber for 4 h to exfoliate the particles. The resulting particles are centrifuged at 5000 and 12000 rpm for 15 min. Subsequently, the collected silicene is dried in a vacuum furnace. To prepare the PPy:

silicone composite, 5 mg of PPy and 5 mg of silicone are added to 4 mL of DMF solution and mixed for 72 h. The layer is fabricated by spin-coating 50 μL of the solution on pre-cleaned and Al back-contacted Si wafers. Coating process is performed at 1500 rpm and 40 s. Following this deposition step, 80 nm thick Al metal is thermally evaporated on the front side of the Ppy:silicene coated side of the device. In this process, a shadow mask is used to specify front rectifying contact area as about 7.85×10^{-3} cm^2. Fig. 1 shows a schematic energy band diagram of the obtained device. As seen in this diagram, PPy has low band energy (Eg = 2.9 eV); as a result, it can be activated in visible light [54,55]. The band structure of silicene (in the absence of spin–orbit interaction) has a zero gap at the Fermi energy, and the work function of silicene is 4.59 eV [56–58]. The calculated band gap energies for the prepared silicene are 0.84 eV and 1.59 eV for indirect and direct transitions from the Kubelka–Munk function.

3. Results and discussion

X-ray diffraction (XRD) analysis is performed to determine the crystal structure of silicene and whether there is contamination due to chemical processes. The obtained XRD pattern of the silicene is presented in Fig. 2a. The crystal structure properties of silicene affect its electrical properties. Contamination in silicene adversely affects the electrical performance of silicene [59]. The diffraction peaks indicate orientations from right to left as (311), (220), and (111), which can be attributed to centrosymmetric cubic crystals in the Fd-3m (227) space group. In addition to the XRD peaks of silicene, there is no pattern belonging to any other element observed. This experimental result confirms the structure of silicene and indicates its consistency with JCPDS Card No. 73–1665 database. It also shows the high purity of silicene. As a result of this evaluation, it is determined that each edge forms 5.431 Å long cubic cell. The structure of the obtained silicene is cF8 silicene, which is the 2D allotrope of silicon. Studies of different phases of silicon show that the cF8 form is more stable [60]. To determine the fundamental optical properties, the energy band gap, Ultraviolet-Visible (UV–Vis) diffuse reflectance spectroscopy is performed. UV–Vis spectroscopy provide information on the optical properties of silicene, which is important for understanding the interaction of materials with light and their energy levels with possible contamination due to chemical processes. The light absorption properties of silicene at specific wavelengths have an impact on its potential applications. It enables determine the energy band gap of silicene, which affects the electrical properties of silicene. Moreover, it can also provide information on purity of silicene. If unexpected absorption peaks are observed at

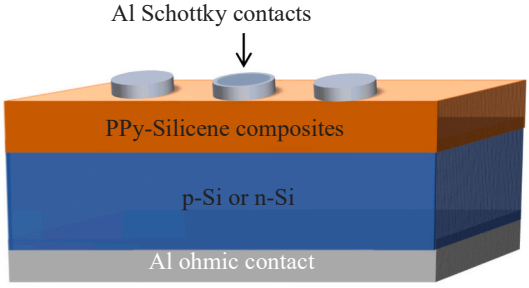

(a)

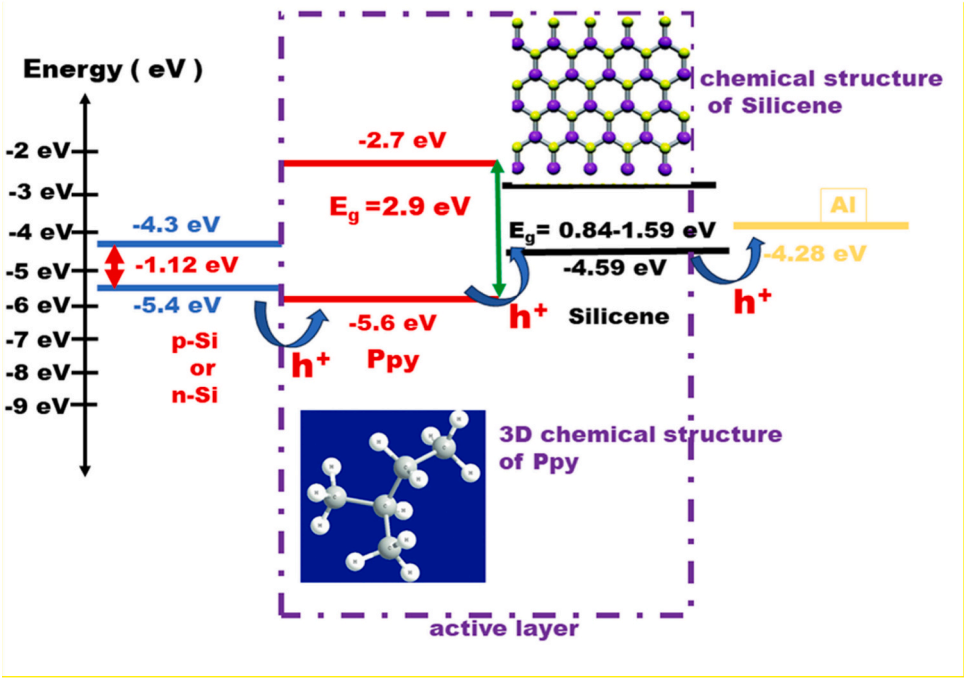

(b)

Fig. 1. (a) a Schematic illustration and (b) energy band diagram of Al/PPy-silicene/p-Si or n-Si devices.

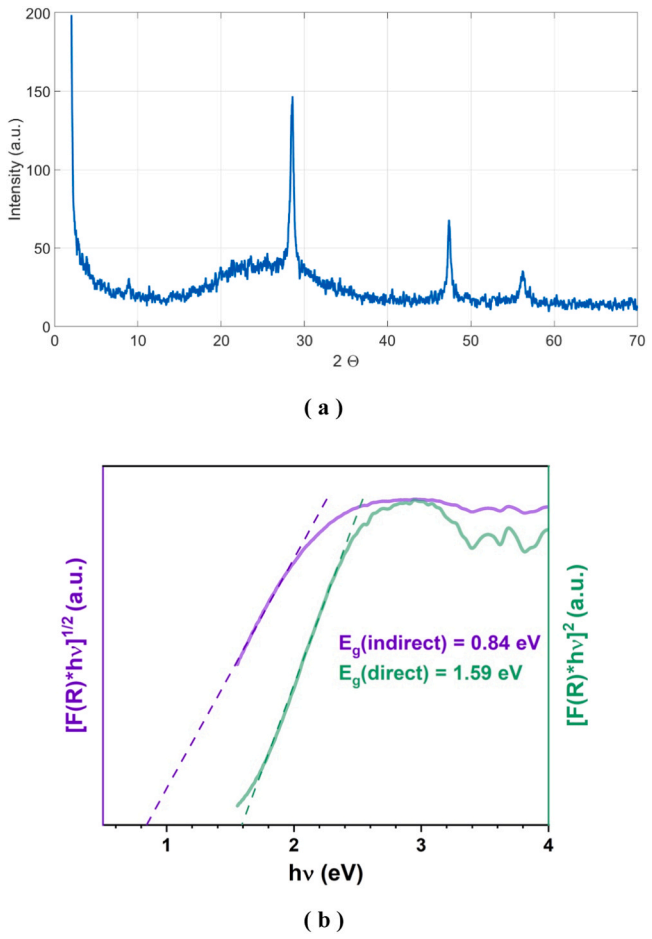

Fig. 2. (a) XRD diffractogram and (b) the Tauc plots of Kubelka-Munk function for both direct and indirect band gaps of silicene materials.

certain wavelengths, this may indicate the presence of contaminants [61]. The spectroscopic measurement is performed to calculate band gap energies derived from the Kubelka–Munk function with the formula:

$$F(R) = \frac{(1-R)^2}{2R} \tag{1}$$

where R represent the diffuse reflectance obtained from the spectroscopy measurements.

A Tauc plot is a graph used to determine the energy band gap of a semiconductor material from optical absorption measurements. The difference between the upper band gap and the lower band gap determines the semiconducting properties of the material. This plot usually plots the relationship between α (absorption coefficient) and the energy E. Only absorption data at specific wavelengths are used. The absorption coefficient usually shows a relationship of the form $\alpha \propto (E-Eg)n$, where Eg is the energy band gap and n represents the type of transition (e.g., n=1/2 for direct transitions, n=2 for indirect transitions) [61]. The Tauc plot of this function is drawn to obtain both direct and indirect band gap transitions of the silicene sample (Fig. 2b). The calculated band gap energies for the prepared silicene are 0.84 eV and 1.59 eV for indirect and direct transitions, respectively. These low band gap energies play important roles for the electrical devices and optoelectronic applications by ensuring high conductivity to results elevated output current of the photodiodes.

Since metal-semiconductor contacts are the primary structure of the fabricated photodiodes, electrical characterization is crucial for the performance and functionality of these devices. [62,63]. At this point of view, there is a conventional tendency to construct Si-based junctions. It is a well-known semiconducting material so that it can provide more predictable ways to analyze final diode characteristics. It also cost-effective materials with high thermal stability and low leakage current [64,65]. In most electronic applications, it is preferred to high-power industrial devices in large-scale production due to getting with well-established processes. The use of heterostructures in n-Si and p-Si is also essential for improving device performance according to engineering availability in band alignment, carrier transport and recombination loses [65–67]. Therefore, the current-voltage ($I-V$) measurements for the prepared diodes are conducted under dark and at room temperature. Additionally, these measurements are performed under various light intensities to determine the light sensitivity of the diodes. The obtained results are given in Fig. 3 for detailed observation of current behavior against varying voltage.

The forward and reverse $I-V$ characteristics of the Ppy:silicene/n-Si and Ppy-silicene/p-Si devices are given in Fig. 3a and b, respectively. The increase in current values depending on increasing voltage and light intensity is clearly observed in these figures both in reverse and forward voltage regions. The higher-than-expected reverse bias current can be related to the conductivity level of the interfacial layer material and to the rectifying behavior capabilities of the materials used [68,69]. Furthermore, according to Fig. 3, the devices present highlight responsivity of the devices to change in light intensity [70].

These plots show achievement to rectifying behavior in the devices, that allows currents to flow in the positive voltage region while blocks in the negative voltage region (reverse bias). The ratio between forward and reverse bias currents are calculated to indicate rectification ratios and the results are presented in Fig. 4a and b, for Ppy:silicene/n-Si and Ppy:silicene/p-Si photodiodes, respectively. As seen from these obtained plots, the rectification ratio of Ppy:silicene/p-Si device is significantly higher than that of device Ppy:silicene/n-Si. This situation can be attributed to the fact that the p-Si material forming a more favorable contact with Al metal. The rectifying behavior can be analyzed by conventional thermionic emission model in which potential contributions from various transport mechanisms are disregarded [71,72]. It can be used to determine characteristic diode parameters from $I-V$ data and so that these results obtained under different conditions can be compared to evaluate diode response. Thus, the dark and illuminated $I-V$ plots are examined to get detailed characterization of the devices. As seen in Fig. 3, exposure to illumination leads to rise of minority charge carriers within the diode, leading to generation of photocurrent. At the region of the reverse bias polarization, the current magnitude is observed to be increased from dark to higher light intensities. This characteristic behavior proves the light sensitivity of the fabricated diode and highlights increase in this response with light intensity. As a result of these observations, the fabricated devices are found in photo-responsive properties [73].

Thermionic emission method widely used to obtain diode ideality (n) and barrier height (Φ_b) and its standard formulation is as follows [64,65,73]:

$$I = I_0 \exp\left(\frac{qV}{nkT}\right)\left[1-\exp\left(-\frac{qV}{kT}\right)\right] \tag{2}$$

where I_0 is named as reverse saturation current, which depends on the Richardson constant (A^*), with values of 32 A/cm^{2}K^2 for p-type Si [59] and 112 A/cm^{2}K^2 for n-type Si [65,74], ambient temperature (T), Boltzmann constant (k), and active device area (A).

$$I_0 = AA^*T^2\exp\left(-\frac{q\Phi_b}{kT}\right) \tag{3}$$

The I_0 values are obtained from the semi-logarithmic $I-V$ plots of the Al/Ppy–silicene/n-Si and Al/Ppy–silicene/p-Si photodiodes (Fig. 3). These values vary with type of the Si material depending on their different work functions where they are 4.3, 4.6, and 4.1 eV for Al, n-Si, and p-Si, respectively. Another well-known fact is that for rectifying

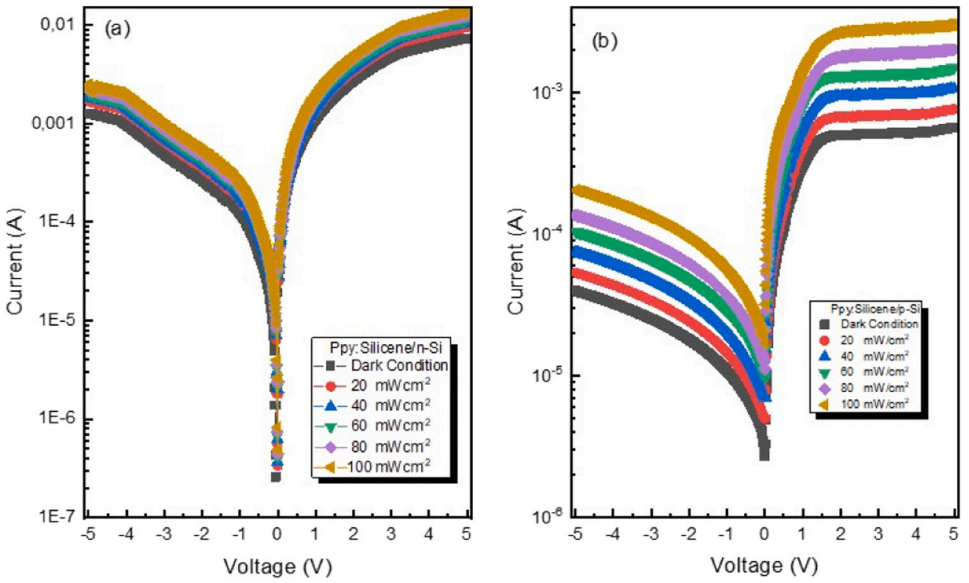

Fig. 3. Semi-logarithmic $I-V$ properties of (a) Ppy:silicene/n-Si and (b) Ppy:silicene/p-Si photodiodes.

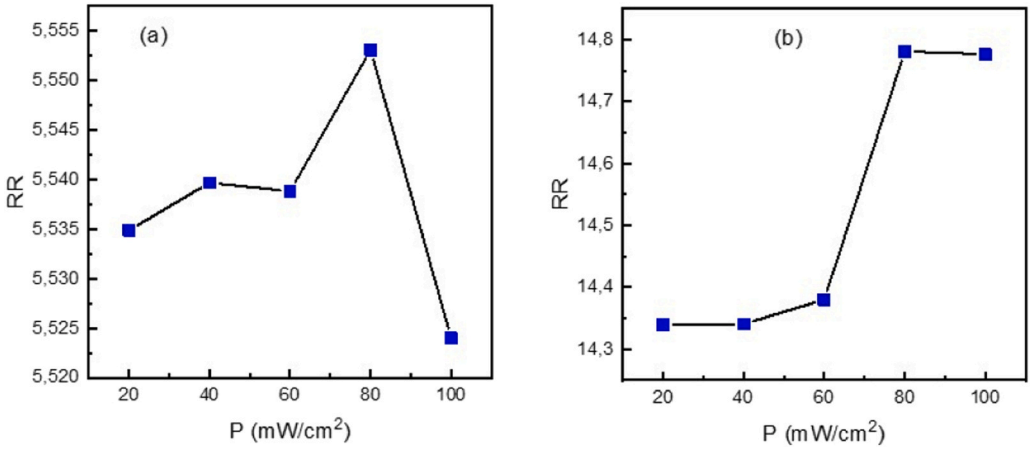

Fig. 4. Rectification ratios of (a) Ppy:silicene/n-Si and (b) Ppy:silicene/p-Si photodiodes.

contact formation, the work function of the semiconductor must be lower than that of the metal contact. Therefore, creating a rectifying contact between n-Si) and Al is challenging. However, it is possible to create a barrier that prevents electrons from easily passing between these two layers. This barrier can be formed either by deposition of interface material between them or by allowing a natural oxide layer to develop on Si surface. Thus, this barrier gives the device rectifying properties, enabling it to control the direction of electron flow, similar to a diode [33,75]. Through the mathematical rearrangement of Eqs. 2 and 3, the diode parameters can be calculated from Eqs. 4 and 5 [76].

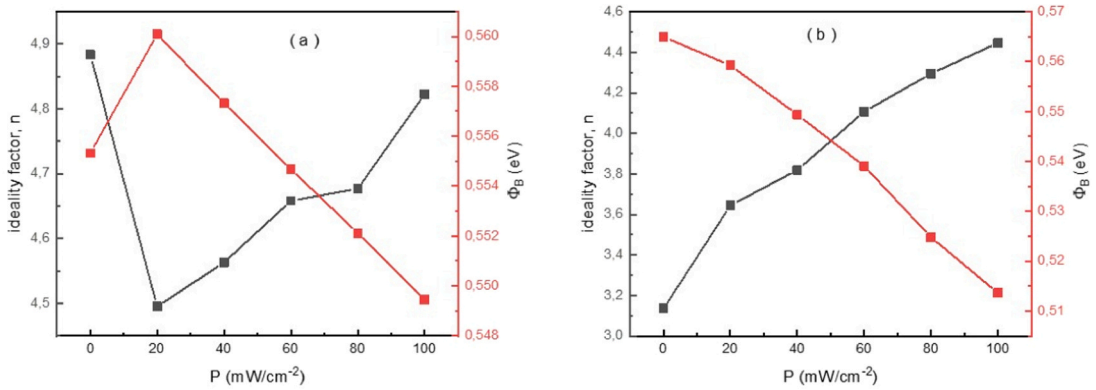

Fig. 5. The ideality factor and barrier height values against to voltage data of (a) Ppy:silicene/n-Si and (b) Ppy:silicene/p-Si photodiodes.

$$\Phi_b = \frac{kT}{q}\ln\left(\frac{A^*AT^2}{I_0}\right) \quad (4)$$

$$n = \frac{q}{kT}\left(\frac{dV}{dlnI}\right) \quad (5)$$

The n values are determined by analyzing the slope of the linear region (Eq. 5) of the $I-V$ graphs and Φ_b values are found from their extrapolation on V-axis. Fig. 5a displays the electrical parameter values of the Ppy:silicene/n-Si device, and Fig. 5b presents the data for the Ppy: silicene/p-Si device. The characteristics of the device based on p-Si indicate that n values increase with increasing light intensity whereas this change decreases Φ_b values Additionally, the device formed on n-Si shows that n values decrease from approximately 4.9 to 4.5 at initial illumination condition. However, these values increase following to increasing in light intensity. On the other hand, Φ_b values of this diode exhibit the opposite behavior compared to them. The values of the Ppy: silicene/p-Si given in Fig. 5b verify proper device operation in this structure due to the compatibility between the work functions of the used metal and semiconductor. However, n value of the device fabricated using p-Si substrate is approximately 3.1 under dark conditions, whereas it is found approximately as 4.9 for the device based on n-Si. Therefore, it can be stated that the device with p-Si substrate and Ppy: silicene interfacial layer exhibits behavior closer to an ideal diode than the other diode structure. Furthermore, as evident from both graphs (Fig. 5), n value is significantly higher than the value required for an ideal diode ($n = 1$). It can be related to a variety of factors, including series resistance, recombination effects, irregularities at the barrier interface, and conditions affecting the interface [77,78]. These results reveal that charge transport across the junction interface is under effect of thermionic emission transport mechanisms in the conduction [79,80]. The calculated n values are higher than 2 and it generally indicates that mechanisms as recombination, tunneling, or space-charge-limited conduction are in effective roles in the charge transport. Thus, space charge limited current (SCLC) mechanism can be supporting mechanism under the effect of traps in the structure [81]. In addition, possible defects in the structures may increase the interface states, which result in inhomogeneity and deviation from ideality [82]. The ideality factor of these diodes is found higher than 2 that can be related to dominant effect of hetero face on the diode's recombination. Depending on the charge motion between trap assisted tunnels, defect recombination and generation of weak photo-generating charge carriers, this factor can be resulted in these high values [83–86]. Therefore, according to these results, the device based on p-Si leads to more efficient device performance and better output characteristics. On the other hand, the decrease in Φ_b values can be associated with an increase in both photocurrents and saturation currents of the diodes. Under increased light intensity, electrons in the structure can gain enough energy to move freely. This increased movement of electrons reduces the threshold energy barrier that usually restricts their flow [87]. In addition, the behavior of the current values under the reverse bias of the devices produced also differed. The linear increase in reverse current without saturation suggests that the device operates predominantly in the photogenerated current regime. The absence of soft saturation or breakdown effects implies that the applied reverse bias is below the threshold for avalanche breakdown, allowing for continuous charge carrier collection with increasing bias voltage.

These parameters can also be derived from Cheung's method [88]. Modeling $I-V$ data by this approach, series resistance (R_s) are calculating in addition to$n$ and Φ_b values. Voltage region of interest is the main difference between this method and the thermionic emission method. Unlike thermionic emission model, the current values from the high voltage region known as the series resistance region where the current deviates from linearity, are used in the evaluations [89]. The $I-V$ equation in Cheung analysis is essentially derived from Eq.1 [64, 65] as;

$$I = I_0\exp\left(-\frac{q(V-IR_s)}{nkT}\right) \quad (6)$$

Different from Eq.1, this current equation includes the IR_s term representing the voltage drop across the device due to the existence of R_s. Related to this approach, Cheung functions can be found as [90];

$$\frac{dV}{d(\ln I)} = IR_s + n\frac{kT}{q} \quad (7)$$

$$H(I) = V - \frac{nkT}{q}\ln\left(\frac{I}{AA^*T^2}\right) = IR_s + n\Phi_b \quad (8)$$

According to these functions, the obtained characteristic plots for Ppy:silicene interlayered devices based on n-type and p-type Si are presented in Fig. 6a and b, separately. These equations gives in linear relations in between the variables linearity; hence the data curves are exhibited as in linear behaviors. The reasons for using two Cheung functions are to reach diode parameters as well as consistency controlling the obtained values. While R_s and Φ_b are calculated from the $H(I)-I$ graph, R_s and n are found from the $dV/dlnI-I$ graph (Fig. 7). Using Eq.7, the n values are obtained as 5.13 for the device based on n-type Si and 3.04 for the device based on p-type Si. Additionally, the Φ_b values are determined as to be 0.563 eV for the n-type Si-based device and 0.559 eV for the p-type Si-based device. These obtained values differ those found through thermionic emission analysis due to the regions of data used, despite being approximately consistent. In the evaluation of the n-type Si-based Ppy-silicene interface-layered device, the R_s value obtained from the $H(I)$ graph is about 11.8 kΩ, whereas this parameter obtained from the $dV/dlnI$ graph is in a values close to 12.6 kΩ. Additionally, for the p-type Si-based device, this value obtained from $H(I)$ is 6.4 kΩ, while from the $dV/dlnI$ graph it is found to be 6.7 kΩ. The main reason for the values obtained for the n-Si-based device being larger compared to those obtained for the p-Si-based device can be attributed to the difference in barrier inhomogeneity between the semiconductor and metal, as well as the influence of interface states [14,90].

Transient photocurrent measurements are essential tools in investigating the performance characteristics and dynamic behavior of a photodiode. These measurements are used to examine the impact of external stimulus light, which is crucial for photonic applications of the fabricated devices. These measurements are performed for both of the fabricated and their response are presented in Fig. 7a and b, respectively. The results show that there is a transition from high to low conductivity when the light is turned off, and high conductivity when turned on again. Under illumination, photocurrent is generated immediately, leading significant increase in the number of charge carriers. This causes total current rise until reaching a certain point, where it stabilizes. Subsequently, when the light source is deactivated, the current rapidly decreases back towards its initial level. This swift decline in photocurrent can be attributed to the trapping of charge carriers at deep levels [91,92]. This evaluation of the measurement data involves two crucial parameters; photoresponse magnitude and its duration. From I_{on}/I_{off} ratio, the photoresponse values of the produced n-type and p-Si semiconductor-based devices are found to be 29 and 173, respectively. This result indicates that the photoresponse value of the photodiode with the Ppy-silicene/p-Si structure is approximately 6 times greater than that of the Ppy-silicene/n-Si photodiode. In addition to the photoresponse value, the rise and fall times are also been investigated from Fig. 7. While the rise time of a detector is defined a time of the increase at the current between the 10 % and 90 % of its maximum value, the fall time shows a time of decrease at the current 90 % and 10 % of its maximum value. The rise (fall) time for the n-type Si-based device is measured as to be 0.054 (0.065) seconds, while for the p-type Si-based device it is 0.028 (0.036) seconds.

Another crucial variable in analyzing a generated photodetector is the photoresponse mechanism in the device. To ascertain the predomi-

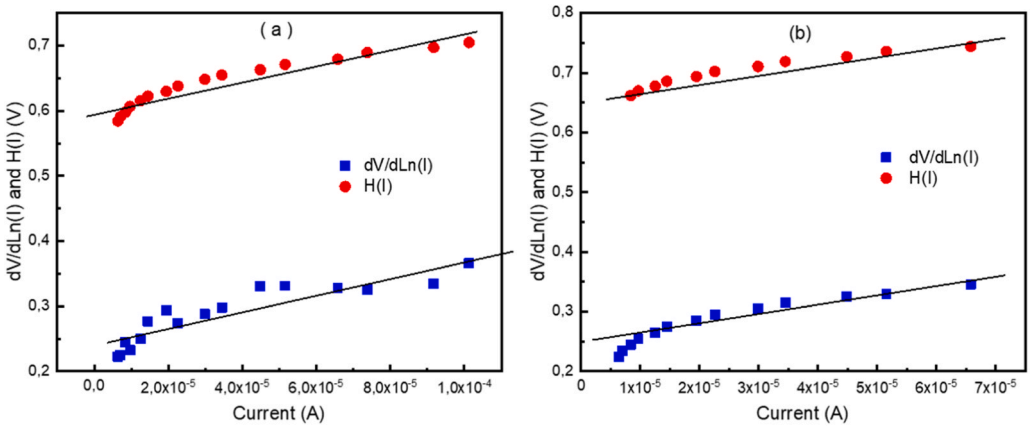

Fig. 6. Cheung curves of the fabricated (a) Ppy:silicene/n-Si and (b) Ppy:silicene/p-Si photodiodes.

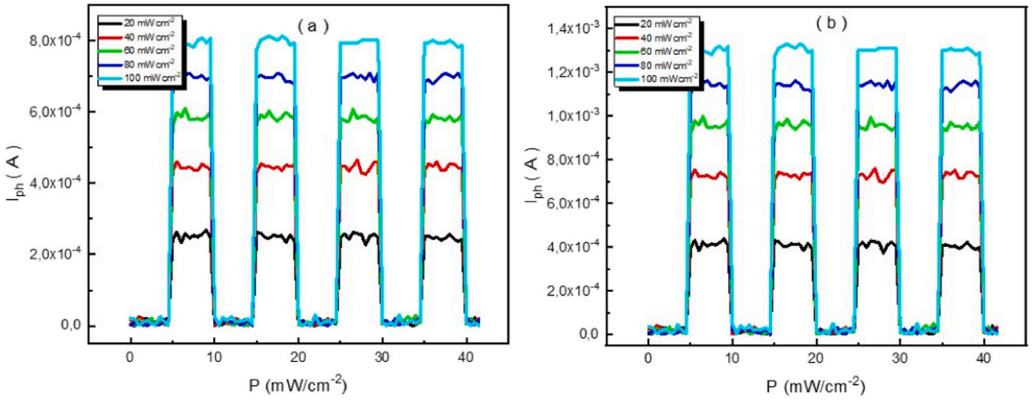

Fig. 7. Transient photocurrent measurements of the generated (a) Ppy:silicene/n-Si and (b) Ppy:silicene/p-Si photodiodes.

nant mechanism affected on photoresponse behavior, it is necessary to analyses the photoresponse value for each light intensity. The related graph plotted in a relation of the measured photocurrent values against the light intensity is shown in Fig. 8. When interpreting this graph, the following power law can be used to express the relationship between photocurrent and exposed light intensity [93].

$$I_{ph} = \beta P^{\alpha} \tag{9}$$

The variable in this equation is the measured photocurrent (I_{ph}) where it is mainly dependent on the applied luminous power P. The parameters β and α denote a constant and the exponent of the relation, respectively. From the gradient of the graph, the values of α are calculated at −2 V bias value. It is expected to equal to or greater than 1, fall within the range of 0.5–1. These values help determine the mechanism that effectively transmits the photocurrent [94]. The calculations for the Ppy-silicene/n-Si and Ppy/p-Si photodiodes are resulted in values of α as 0.612 and 1.414, respectively. The obtained value is greater than 1 for the p-type Si-based device, indicating that the localized states are appropriately positioned within the mobility gap. On the other hand, the value obtained for the n-type Si-based device is less than 1, which signifies the presence of localized traps [95]. As observed Fig. 8, the photocurrent increases directly proportional to the intensity of illumination, which refers that photogeneration is correlated with the number of photons adsorbed by the device [96,97].

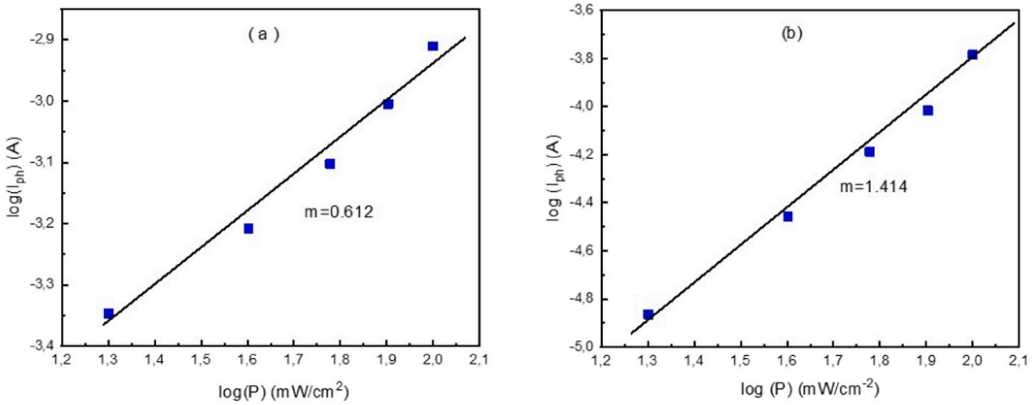

Fig. 8. log (I_{ph}) - log (P) graph of the manufactured (a) Ppy:silicene/n-Si and (b) Ppy:silicene/p-Si photodiodes.

There are parameters to provide a more comprehensive presentation of the device performance under light in addition to the sensitivity of the device to illumination. Therefore, essential detector parameters can be determined using transient photocurrent experiments. The sensitivity (R), specific detectivity (D^*), and photocurrent (I_{ph}) values of the device with the n- and p-type Si are obtained using the following equations [98,99].

$$R = I_{ph}/PA \tag{10}$$

$$D^* = R\sqrt{\frac{A}{2qI_{dark}}} \tag{11}$$

The responsivity of a photodevice represents the relationship between the generated photocurrent and the absorbed/incident optical power. In photodiodes, responsivity peaks in the wavelength range where photon energy exceeds the band gap energy, and sharply reduces within the band gap zone can be observed due to reduced absorption [99]. Photosensitivity (K) is an essential characteristic parameter that outlines the capability of a photodiode to convert incident light into an electrical signal. It is an indispensable metric for assessing the performance of photodetectors [99–101]. The K values can be determined by dividing I_{ph} by the dark current (I_{dark}) [101].

The experimental values are plotted in Fig. 9 to show the responsivity values of the devices with different substrates. Fig. 9a indicates the characteristics of the Ppy-silicene/n-Si photodiode where responsivity values decrease as the light intensity increases. Conversely, for the device designed with p-Si substrate, it is seen that responsivity increases in with following increase in light intensity (Fig. 9b).

The detectivity values of photodiodes for the fabricated diodes on n-Si and p-Si are illustrated in Fig. 10a and b, respectively. These values are found in the order of 10^9 Jones consistent with the literature [102–105]. As given in these figures, detectivity values vary proportionally with sensitivity values as expected.

4. Conclusion

The PPy-silicene composite material is prepared and deposited as an interfacial layer on n-/p-type Si semiconductors for fabrication of Al/PPy-Silicene/n-Si and Al/PPy-Silicene/p-Si photodiodes. In the XRD analysis, the silicene material is found to be in a crystalline structure. In the diode studies, the diode parameters as barrier height, series resistance, and ideality factor, which reveal the performance level of the device, are analyzed using current-voltage measurements. Thermionic emission and Cheung approaches are employed in detailed analyses. The barrier height (ideality factor) values for the fabricated p-type and n-type Si based devices are calculated as 0.57 eV (3.1) and 0.55 eV (4.9), respectively. Moreover, as an essential analysis for the fabricated devices in photonic application, effects of illumination on the electrical performance, is studied under various light intensities (20, 40, 60, 80, and 100 mW/cm^2) through current-voltage/time measurements. Additionally, detector parameters as sensitivity, detectivity and responsivity, having significant importance for optoelectronic applications, are investigated. The experimental results show that both diode and photodiode performance of the Al/PPy-Silicene/p-Si device is significantly higher than that of the Al/PPy-Silicene/n-Si device. Moreover, it can be concluded that the PPy-Silicene composite material is suitable for use in photodetection.

The charge transport mechanisms in Ppy are based on the motion of radical cations or anions, which are created by oxidation or reduction, along a polymer chain and on charge hopping between neighboring molecules [106–109]. Semiconducting properties of Ppy come from the delocalized π-electron bonding along the polymer chain. Molecular orbitals of the repeated units overlap in space and lift their degeneracy by forming a series of energy bands. Delocalized valance and conduction bands are created by π-bonding and π*-antibonding orbitals, respectively [107–110]. The Fermi level of the Ppy or Ppy:Silicene layer is strongly influenced by the structure, the dopant type and the doping level [110–112]. Hence, the junction characteristic of the metal/PPy and metal/Ppy:Silicene Schottky diodes are strongly influenced by the conditions of preparation [107]. A doping/dedoping process of Ppy or Ppy:Silicene layer can realize the reversible change in Ppy:silicene/n-type or Ppy:silicene/p-type interface. It's known that the insulator-to-metal transition is related to the delocalization of the electronic charge along the polymer backbone. The charging of Ppy or Ppy:Silicene results in the appearance of positively charged species such as polarons or bipolarons [113,114]. Owing to highly controllable properties for synthesis of Ppy, it has been utilized in heterojunction devices as an alternative of conventional inorganic semiconductive/conductive materials in the field of photodetectors and the other devices [109–115].

CRediT authorship contribution statement

D. E. Yıldız: Writing – review & editing, Supervision, Methodology, Investigation. **Abdulkerim Karabulut:** Writing – review & editing, Writing – original draft, Methodology, Investigation, Conceptualization. **A. Gulsaran:** Writing – review & editing, Methodology, Investigation, Conceptualization. **N. Tasaltın:** Methodology, Investigation. **M. Yavuz:** Writing – review & editing, Methodology, Investigation, Conceptualization. **B. Bastug Azer:** Writing – review & editing, Methodology, Investigation, Formal analysis. **M. Yıldırım:** Methodology, Investigation, Formal analysis. **A. Kocyigit:** Methodology, Investigation. **H. H. Güllü:** Writing – review & editing, Investigation, Formal analysis.

Declaration of Competing Interest

The authors declare that they have no known competing financial interests or personal relationships that could have appeared to influence the work reported in this paper.

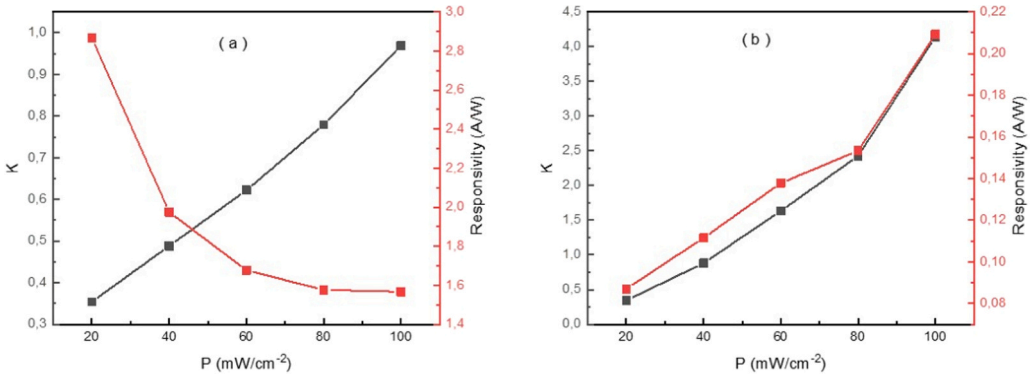

Fig. 9. K and responsivity values of the fabricated (a) Ppy:silicene/n-Si and (b) Ppy:silicene/p-Si photodiodes.

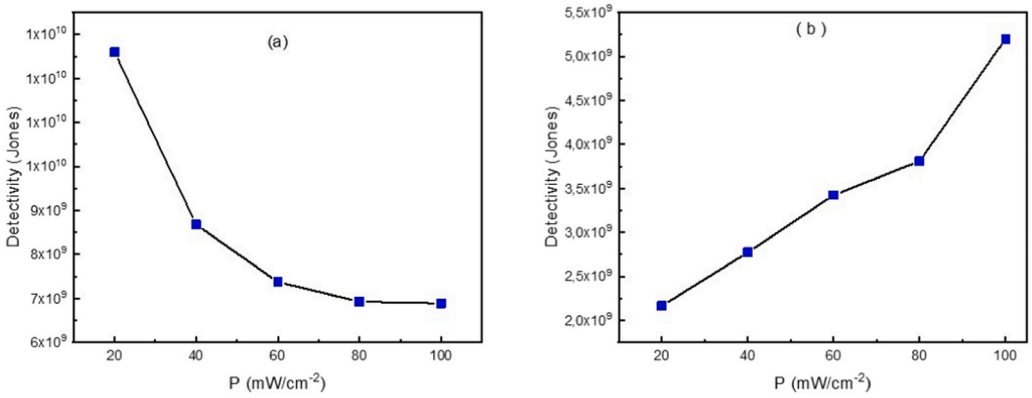

Fig. 10. Specific detectivity values of the generated (a) Ppy:silicene/n-Si and (b) Ppy:silicene/p-Si photodiodes.

Data Availability

Data will be made available on request.

References

[1] Y. Mei, X. Bi, Z. Cao, J. Weng, X. Guo, Q. Xu, Automatic power control for a frequency tunable optoelectronic oscillator, IEEE Trans. Circuits Syst. II Express Briefs 70 (4) (2022) 1385–1389.

[2] Z. Bielecki, T. Stacewicz, J. Wojtas, J. Mikołajczyk, D. Szabra, A. Prokopiuk, Selected optoelectronic sensors in medical applications, Opto-Electron. Rev. 26 (2) (2018) 122–133.

[3] Handbook of optoelectronics: concepts, in: J.P. Dakin, R. Brown, J.P. Dakin, R. Brown (Eds.), Devices, and Techniques (Volume One), CRC press, 2017.

[4] M.H. Hachemi, M. Benchehima, K. Bencherif, H. Abid, The effect of N-incorporation on the structural and optoelectronic properties of GaP and GaAs for optical telecommunication applications: first-principles study, Optik 262 (2022) 169282.

[5] J. Wang, J. Song, X. Mu, M. Sun, Optoelectronic and photoelectric properties and applications of graphene-based nanostructures, Mater. Today Phys. 13 (2020) 100196.

[6] A. Karabulut, İ. Orak, A. Türüt, The photovoltaic impact of atomic layer deposited TiO2 interfacial layer on Si-based photodiodes, Solid-State Electron. 144 (2018) 39–48.

[7] B.N. Pal, I. Robel, A. Mohite, R. Laocharoensuk, D.J. Werder, V.I. Klimov, High-sensitivity p–n Junction photodiodes based on PbS nanocrystal quantum dots, Adv. Funct. Mater. 22 (8) (2012) 1741–1748.

[8] F. Yakuphanoglu, F.S. Shokr, R.K. Gupta, A.A. Al-Ghamdi, S. Bin-Omran, Y. Al-Turki, F. El-Tantawy, A new type photodiode: p-Si/GaN pn junction in series with GaN/Ag Schottky diode, J. Alloy. Compd. 650 (2015) 671–675.

[9] G.A. Sibu, P. Gayathri, T. Akila, R. Marnadu, V. Balasubramani, Manifestation on the choice of a suitable combination of MIS for proficient Schottky diodes for optoelectronic applications: a comprehensive review, Nano Energy 125 (2024) 109534.

[10] R. Singh, A.R. Polu, B. Bhattacharya, H.W. Rhee, C. Varlikli, P.K. Singh, Perspectives for solid biopolymer electrolytes in dye sensitized solar cell and battery application, Renew. Sustain. Energy Rev. 65 (2016) 1098–1117.

[11] D. Nikolić, K. Stanković, L. Timotijević, Z. Rajović, M. Vujisić, Comparative study of gamma radiation effects on solar cells, photodiodes, and phototransistors, Int. J. Photo 2013 (1) (2013) 843174.

[12] P. Gayathri, T. Akila, G.A. Sibu, M. Selvaraj, M.A. Assiri, P. Matheswaran, V. Balasubramani, Enhancing photovoltaic applications through precipitating agents in ITO/CIS/CeO2/Al heterojunction solar cell, Inorg. Chem. Commun. 168 (2024) 112866.

[13] B.A. Gozeh, A. Karabulut, A. Yildiz, F. Yakuphanoglu, Solar light responsive ZnO nanoparticles adjusted using Cd and La Co-dopant photodetector, J. Alloy. Compd. 732 (2018) 16–24.

[14] W.A. Farooq, E. Elgazzar, A. Dere, O. Dayan, Z. Serbetci, A. Karabulut, A. Hanif, Photoelectrical characteristics of novel Ru (II) complexes based photodiode, J. Mater. Sci.: Mater. Electron. 30 (6) (2019) 5516–5525.

[15] J. Cao, S. Fiore, C. Klinkert, N. Vetsch, M. Luisier, Light-matter interactions in van der Waals photodiodes from first principles, Phys. Rev. B 106 (3) (2022) 035306.

[16] C. Wang, X. Zhang, W. Hu, Organic photodiodes and phototransistors toward infrared detection: materials, devices, and applications, Chem. Soc. Rev. 49 (3) (2020) 653–670.

[17] P. Vivek, J. Chandrasekaran, V. Balasubramani, A. Manimekalai, T.G. Vignesh Prabhu, Insertion of Ga-MoO3 thin film at Cu/p-Si interface for the fabrication of MIS structure Schottky barrier diodes, Surf. Inter. 37 (2023) 102689.

[18] A. Karabulut, D.E. Yıldız, D.A. Köse, M. Yıldırım, Photosensing performances of heterojunctions-based photodiodes with novel complex interlayers, Mater. Sci. Semicond. Process. 146 (2022) 106647.

[19] R.D. Jansen-van Vuuren, A. Armin, A.K. Pandey, P.L. Burn, P. Meredith, Organic photodiodes: the future of full color detection and image sensing, Adv. Mater. 28 (24) (2016) 4766–4802.

[20] F. Özel, E. Arkan, H. Coskun, İ. Deveci, M. Yıldırım, M. Yıldırım, M. Ersöz, Refractory-metal-based chalcogenides for energy, Adv. Funct. Mater. 32 (47) (2022) 2207705.

[21] W. Zhang, X. Zhang, L.K. Ono, Y. Qi, H. Oughaddou, Recent advances in phosphorene: structure, synthesis, and properties, Small 20 (4) (2024) 2303115.

[22] I. Oreibi, J.M. Al-ıssawe, A class of two-dimensional WSeTe monolayers under pressures with novel electronic and optical properties, Turk. Comput. Theor. Chem. 7 (2) (2023) 12–19.

[23] G. Shan, H. Tan, R. Ma, H. Zhao, W. Huang, Recent progress in emergent two-dimensional silicene, Nanoscale 15 (7) (2023) 2982–2996.

[24] V.K. Dien, W.B. Li, K.I. Lin, N.T. Han, M.F. Lin, Electronic and optical properties of graphene, silicene, germanene, and their semi-hydrogenated systems, RSC Adv. 12 (54) (2022) 34851–34865.

[25] S. Moon, J. Kim, J. Park, S. Im, J. Kim, I. Hwang, J.K. Kim, Hexagonal boron nitride for next-generation photonics and electronics, Adv. Mater. 35 (4) (2023) 2204161.

[26] F. Bechstedt, P. Gori, O. Pulci, Beyond graphene: clean, hydrogenated and halogenated silicene, germanene, stanene, and plumbene, Prog. Surf. Sci. 96 (3) (2021) 100615.

[27] J. Sone, T. Yamagami, Y. Aoki, K. Nakatsuji, H. Hirayama, Epitaxial growth of silicene on ultra-thin Ag (111) films, N. J. Phys. 16 (9) (2014) 095004.

[28] B. Mortazavi, O. Rahaman, M. Makaremi, A. Dianat, G. Cuniberti, T. Rabczuk, First-principles investigation of mechanical properties of silicene, germanene and stanene, Phys. E: Low. Dimens. Syst. Nanostruct. 87 (2017) 228–232.

[29] J. Zhuang, X. Xu, H. Feng, Z. Li, X. Wang, Y. Du, Honeycomb silicon: a review of silicene, Sci. Bull. 60 (2015) 1551–1562.

[30] L.C. Lew Yan Voon, Physical Properties of Silicene, in: In Springer Series in Materials Science, 235, Springer Verlag, 2016, pp. 3–33.

[31] Umam, K., Nurwantoro, P., Absor, M.A.U., Nugraheni, A.D., & Budhi, R.H. (2018, April). Biaxial Strain Effects on the Electronic Properties of Silicene: the Density-functional-theory-based Calculations. in Journal of Physics: Conference Series (Vol. 1011, No. 1, p. 012074). IOP Publishing.

[32] X. Yang, J. Ni, Electronic properties of single-walled silicon nanotubes compared to carbon nanotubes, Phys. Rev. B 72 (2005) 195426, https://doi.org/10.1103/PhysRevB.72.195426.

[33] A. Kocyigit, D.E. Yıldız, N. Taşaltın, M. Yıldırım, Role of interfacial layer as PANI–silicene in Si-based photodiodes, J. Mater. Sci. (2024) 1–18.

[34] M.A. Kharadi, G.F.A. Malik, K.A. Shah, F.A. Khanday, Performance analysis of functionalized silicene nanoribbon-based photodetector, Int. J. Numeric. Model. Electron. Netw. Dev. Fields 34 (1) (2021) e2809.

[35] F. Gao, N. Zhang, X. Fang, M. Ma, Bioinspired design of strong, tough, and highly conductive polyol-polypyrrole composites for flexible electronics, ACS Appl. Mater. Interfaces 9 (7) (2017) 5692–5698.

[36] G.B. Street, S.E. Lindsey, A.I. Nazzal, K.J. Wynne, The structure and mechanical properties of polypyrrole, Mol. Cryst. Liq. Cryst. 118 (1) (1985) 137–148.

[37] A.F. Diaz, J.I. Castillo, J.A. Logan, W.Y. Lee, Electrochemistry of conducting polypyrrole films, J. Electroanal. Chem. Interfacial Electrochem. 129 (1-2) (1981) 115–132.

[38] R. Jain, N. Jadon, A. Pawaiya, Polypyrrole based next generation electrochemical sensors and biosensors: a review, TrAC Trends Anal. Chem. 97 (2017) 363–373.

[39] S. Carquigny, J.B. Sanchez, F. Berger, B. Lakard, F. Lallemand, Ammonia gas sensor based on electrosynthesized polypyrrole films, Talanta 78 (1) (2009) 199–206.

[40] P.S. Thapa, D.J. Yu, J.P. Wicksted, J.A. Hadwiger, J.N. Barisci, R.H. Baughman, B. N. Flanders, Directional growth of polypyrrole and polythiophene wires, Appl. Phys. Lett. 94 (3) (2009).

[41] E.W. Jager, E. Smela, O. Inganas, I. Lundstroem, Applications of Polypyrrole Microactuators, in: In Smart Structures and Materials 1999: Electroactive Polymer Actuators and Devices, 3669, SPIE, 1999, May, pp. 377–384.

[42] H. Xie, D. Ma, L. Zhang, A PPy modified Al2O3-mullite coating on Al alloys for anti-static electricity and corrosion resistance, Ceram. Int. 49 (11) (2023) 18885–18895.

[43] Y. Kudoh, T. Kojima, M. Fukuyama, S. Tsuchiya, S. Yoshimura, Covering anodized aluminum with electropolymerized polypyrrole via manganese oxide layer and application to solid electrolytic capacitor, J. Power Sources 60 (2) (1996) 157–163.

[44] M. Bayat, H. Izadan, S. Santiago, F. Estrany, M. Dinari, D. Semnani, G. Guirado, Study on the electrochromic properties of polypyrrole layers doped with different dye molecules, J. Electroanal. Chem. 886 (2021) 115113.

[45] Q. Gao, M. Lei, K. Zhou, X. Liu, S. Wang, H. Li, Preparation of a microfibrillated cellulose/chitosan/polypyrrole film for active food packaging, Prog. Org. Coat. 149 (2020) 105907.

[46] S. Kakuda, T. Momma, T. Osaka, G.B. Appetecchi, B. Scrosati, Ambient-temperature, rechargeable, all-solid lithium/polypyrrole polymer battery, J. Electrochem. Soc. 142 (1) (1995) L1.

[47] Y. Huang, H. Li, Z. Wang, M. Zhu, Z. Pei, Q. Xue, C. Zhi, Nanostructured polypyrrole as a flexible electrode material of supercapacitor, Nano Energy 22 (2016) 422–438.

[48] M.M. Perez-Madrigal, L.J. Del Valle, E. Armelin, C. Michaux, G. Roussel, E. A. Perpete, C. Alemán, Polypyrrole-supported membrane proteins for bio-inspired ion channels, ACS Appl. Mater. Interfaces 7 (3) (2015) 1632–1643.

[49] P. Bocchetta, D. Frattini, M. Tagliente, F. Selleri, Electrochemical deposition of polypyrrole nanostructures for energy applications: a review, Curr. Nanosci. 16 (4) (2020) 462–477.

[50] S.M. Amorim, G. Steffen, S. de, J.M. Junior, C.Z. Brusamarello, A.P. Romio, M. D. Domenico, Synthesis, characterization, and application of polypyrrole/TiO2 composites in photocatalytic processes: a review, Polym. Polym. Compos. 29 (7) (2021) 1055–1074.

[51] A.L. Pang, A. Arsad, M. Ahmadipour, Synthesis and factor affecting on the conductivity of polypyrrole: a short review, Polym. Adv. Technol. 32 (4) (2021) 1428–1454.

[52] E.N. Zare, T. Agarwal, A. Zarepour, F. Pinelli, A. Zarrabi, F. Rossi, P. Makvandi, Electroconductive multi-functional polypyrrole composites for biomedical applications, Appl. Mater. Today 24 (2021) 101117.

[53] M.K. Zadeh, M. Yeganeh, M.T. Shoushtari, A. Esmaeilkhanian, Corrosion performance of polypyrrole-coated metals: a review of perspectives and recent advances, Synth. Met. 274 (2021) 116723.

[54] G. Baytemir, N. Tasaltın, B. Karaca, S. Karakus, G. Gursu, B. Barıs, D.E. Yıldız, PANI: silicene nanocompositesbased non-enzymatic electrochemical voltammetric sensor for dopamine detection, J. Mater. Sci. Mater. Electron 34 (2023) 1–10.

[55] S. Zeynali, M.T. Taghizadeh, Highly efficient TiO2/ AgBr/PANI heterojunction with enhanced visible light photocatalytic activity towards degradation of organic dyes, J. Mater. Sci. Mater. Electron 30 (2019) 17020–17031.

[56] H. Liu, J. Gao, J. Zhao, Silicene on substrates: a way to preserve or tune its electronic properties, J., Phys. Chem. C 117 (2013) 10353–10359.

[57] H. Liu, J. Gao, J. Zhao, Silicene on substrates: interaction mechanism and growth behavior, J. Phys. Conf. Ser. 491 (2014) 012007.

[58] W.Q. Huang, S.R. Liu, H.Y. Peng, X. Li, Z.M. Huang, Synthesis of new silicene structure and its energy band properties, Chin. Phys. B 29 (2020) 084202.

[59] T. Akila, P. Gayathri, G.A. Sibu, V. Balasubramani, H. Al-Lohedan, D.M. Al-Dhayan, Augmented photovoltaic performance of Cu/Ce-(Sn: Cd)/n-Si Schottky barrier diode utilizing dual-doped Ce-(Sn: Cd) thin films, Opt. Mater. 149 (2024) 115133.

[60] C. Grazianetti, E. Cinquanta, L. Tao, P. De Padova, C. Quaresima, C. Ottaviani, A. Molle, Silicon nanosheets: crossover between multilayer silicene and diamond-like growth regime, ACS Nano 11 (3) (2017) 3376–3382.

[61] P. Makuła, M. Pacia, W. Macyk, How to correctly determine the band gap energy of modified semiconductor photocatalysts based on UV–Vis spectra, J. Phys. Chem. Lett. 9 (23) (2018) 6814–6817.

[62] A. Karabulut, M. Unlu, M. Yıldırım, D.A. Köse, M.O. Erdal, D.E. Yıldız, Semiconductor-based photodiodes with Ni and Zn-centered nicotinates interfacial layers, J. Mater. Sci. Mater. Electron. 35 (5) (2024) 362.

[63] A.G. Al-Sehemi, A. Tataroğlu, A. Dere, A. Karabulut, A.A. Al-Ghamdi, F. Yakuphanoğlu, The structural, electrical, and photoelectrical properties of Al/Cu2CdSnS4 chalcogenide film/p-Si Schottky-type photodiode, J. Mater. Sci. Mater. Electron. 34 (30) (2023) 2024.

[64] B.L. Sharma, R.K. Purohit, Semiconductor Heterojunctions, Pergamon Press, Oxford/New York/Toronto/Sydney, 1974.

[65] S.M. Sze, K.N. Ng, Physics of Semiconductor Devices, Wiley, Canada, 2007.

[66] G. Ozel, S. Demirezen, Investigation of hybrid CuPc-doped ZnO/p-silicon photodiodes for photonic and electronic applications, J. Mater. Sci. Mater. Electron. 35 (2024) *946*.

[67] S. Demirezen, S. Altindal Yeriskin, A detailed comparative study on electrical and photovoltaic characteristics of Al/p-Si photodiodes with coumarin-doped PVA interfacial layer: the effect of doping concentration, Polym. Bull. 77 (2020) *49–71*.

[68] M. Yilmaz, N. Canpolat, S. Aydoğan, Surface plasmon resonance effects of Ag@ ZnO core–shell nanostructure in UV and visible light for photodiode applications, J. Am. Ceram. Soc. 107 (5) (2024) 3390–3402.

[69] Z. Çaldıran, Ş. Aydoğan, Effects of the photoactive layer properties and current transmission mechanism on optical and electrical characteristics of organic photovoltaic, Optik 241 (2021) 166937.

[70] D.E. Yıldız, A. Karabulut, M. Yıldırım, The influence of light and temperature stimuli on the characteristics of Au/ZnO/n-Si Schottky-type device, J. Mater. Sci. Mater. Electron. 34 (36) (2023) 2272.

[71] A. Karabulut, Barrier height modification in Au/Ti/n-GaAs devices with a HfO 2 interfacial layer formed by atomic layer deposition, Bull. Mater. Sci. 42 (1) (2019) 5.

[72] Ş. Karataş, Ş. Altındal, A. Türüt, A. Özmen, Temperature dependence of characteristic parameters of the H-terminated Sn/p-Si (1 0 0) Schottky contacts, Appl. Surf. Sci. 217 (1-4) (2003) 250–260.

[73] A.D.E.M. Tataroğlu, C. Ahmedova, G. Barim, A.G. Al-Sehemi, A. Karabulut, A. A. Al-Ghamdi, F. Yakuphanoglu, Electronic and optoelectronic properties of Al/coumarin doped Pr 2 Se 3–Tl 2 Se/p-Si devices, J. Mater. Sci. Mater. Electron. 29 (2018) 12561–12572.

[74] E. Aldırmaz, A. Tataroğlu, A. Dere, M. Güler, E. Güler, A. Karabulut, F. Yakuphanoglu, Cu-Al-Mn shape memory alloy based Schottky diode formed on Si, Phys. B Condens. Matter 560 (2019) 261–266.

[75] D.E. Yıldız, Ş. Altındal, Z. Tekeli, M. Özer, The effects of surface states and series resistance on the performance of Au/SnO2/n-Si and Al/SnO2/p-Si (MIS) Schottky barrier diodes, Mater. Sci. Semicond. Process. 13 (1) (2010) 34–40.

[76] D.E. Yıldız, A. Karabulut, I. Orak, A. Turut, Effect of atomic-layer-deposited HfO 2 thin-film interfacial layer on the electrical properties of Au/Ti/n-GaAs Schottky diode, J. Mater. Sci. Mater. Electron. 32 (2021) 10209–10223.

[77] M.A. Mayimele, J.P.J. van Rensburg, F.D. Auret, M. Diale, Analysis of temperature-dependant current–voltage characteristics and extraction of series resistance in Pd/ZnO Schottky barrier diodes, Phys. B Condens. Matter 480 (2016) 58–62.

[78] A. Tataroğlu, Ş. Altındal, Y. Azizian-Kalandaragh, Comparison of electrical properties of MS and MPS type diode in respect of (In2O3-PVP) interlayer, Phys. B Condens. Matter 576 (2020) 411733.

[79] V. Balasubramani, P.V. Pham, A. Ibrahim, J. Hakami, M.Z. Ansari, T.K. Le, Enhanced photosensitive of Schottky diodes using SrO interfaced layer in MIS structure for optoelectronic applications, Opt. Mater. 129 (2022) 112449.

[80] V. Balasubramani, J. Chandrasekaran, R. Marnadu, P. Vivek, S. Maruthamuthu, S. Rajesh, Impact of Annealing Temperature on Spin Coated V2O5 Thin Films as Interfacial Layer in Cu/V2O5/n-Si Structured Schottky Barrier Diodes, J. Inorg. Organomet Polym. Mater. 29 (2019) 1533–1547.

[81] A.B. Ulusan, A. Tataroglu, Y. Azizian-Kalandaragh, S. Altindal, On the conduction mechanisms of Au/(Cu2O–CuO–PVA)/n-Si (MPS) Schottky barrier diodes (SBDs) using current–voltage–temperature (I–V–T) characteristics, J. Mater. Sci. Mater. Electron 29 (2018) 159–170.

[82] H. Durmuş, A. Tataroğlu, Ş. Altındal, M. Yıldırım, The effect of temperature on the electrical characteristics of Ti/n-GaAs Schottky diodes, Curr. Appl. Phys. 44 (2022) 85–89.

[83] P. Harishsenthil, J. Chandrasekaran, R. Marnadu, V. Balasubramani, Incorporation of Zn ions on high dielectric HfO2 thin films by spray pyrolysis and fabrication of Al/Zn@HfO2/n-Si Schottky barrier diodes, Sens. Actuators A Phys. 331 (2021) 112725.

[84] T. Sasikala, K. Shanmugasundaram, P. Thirunavukkarasu, P. Vivek, V. Balasubramani, Impact of phase transformation on MoS2 thin flms on high temperature and its concomitant role in In-MoS2/P-Si structured PN junction diodes, Opt. Mater. 131 (2022) 112584.

[85] I. Tascioglu, G. Pirgholi-Givi, S. Altindal Yeriskin, Y. Azizian, Examination on the current conduction mechanisms of Au/n-Si diodes with ZnO–PVP and ZnO/Ag2WO4 –PVP interfacial layers, J. Sol. Gel Sci. Tech. 107 (2023) 536–547.

[86] S.O. Tan, H. Uslu Tecimer, O. Cicek, H. Tecimer, I. Orak, S. Altindal, Electrical characterizations of Au/ZnO/n-GaAs Schottky diodes under distinct illumination intensities, J. Mater. Sci. Mater. Electron. 27 (2016) 8340–8347.

[87] A. Kocyigit, M. Yilmaz, Ü. İncekara, S. Aydogan, H. Kacus, Molecular engineering for donor electron to enhance photodiode properties of Co/n-Si and Co/p-Si structures: the effect of hematoxylin interface, Optik 242 (2021) 167314.

[88] R.O. Ocaya, F. Yakuphanoğlu, Ocaya–Yakuphanoğlu method for series resistance extraction and compensation of Schottky diode I–V characteristics, Measurement 186 (2021) 110105.

[89] H.K. Kaplan, S. Sarsıcı, S.K. Akay, M. Ahmetoglu, The characteristics of ZnS/Si heterojunction diode fabricated by thermionic vacuum arc, J. Alloy. Compd. 724 (2017) 543–548.

[90] İ. Orak, A. Karabulut, E. Yiğit, Ö. Sevgĭlĭ, A. Ruşen, F. Ozel, The diode and photodiode performances of BaZrO3 perovskite-based device under the influence of thermal and light external stimuli, Sens. Actuators A Phys. 337 (2022) 113413.

[91] F. Spadavecchia, S. Ardizzone, G. Cappelletti, L. Falciola, M. Ceotto, D. Lotti, Investigation and optimization of photocurrent transient measurements on nano-TiO 2, J. Appl. Electrochem. 43 (2013) 217–225.

[92] R.C. MacKenzie, C.G. Shuttle, M.L. Chabinyc, J. Nelson, Extracting microscopic device parameters from transient photocurrent measurements of P3HT: PCBM solar cells, Adv. Energy Mater. 2 (6) (2012) 662–669.

[93] A.G. Al-Sehemi, A. Tataroglu, A. Karabulut, A. Dere, A.A. Al-Ghamdi, F. Yakuphanoglu, Optoelectronic and photonic characteristics of Al/p-Si diode with boric acid-doped zinc oxide interlayer, JOM 75 (9) (2023) 3587–3600.

[94] A.G. Al-Sehemi, K. Ocakoglu, M. Ince, A. Karabulut, A.D.E.M. Tataroğlu, A. Dere, F. Yakuphanoglu, The electronic and optoelectronic properties of Al/hydroxymethyl functionalized Zn (II) Pc/p-Si photonic device, Polym. Bull. 81 (5) (2024) 4351–4368.

[95] A. Mekki, R.O. Ocaya, A. Dere, A.A. Al-Ghamdi, K. Harrabi, F. Yakuphanoglu, Organic semiconductor: graphene-oxide/p-Si photodiodes, J. Nanoelectron. Optoelectron. 11 (2) (2016) 153–163.

[96] M. Buscema, J.O. Island, D.J. Groenendijk, S.I. Blanter, G.A. Steele, H.S. van der Zant, A. Castellanos-Gomez, Photocurrent generation with two-dimensional van der Waals semiconductors, Chem. Soc. Rev. 44 (11) (2015) 3691–3718.
[97] Q. Zhao, W. Wang, F. Carrascoso-Plana, W. Jie, T. Wang, A. Castellanos-Gomez, R. Frisenda, The role of traps in the photocurrent generation mechanism in thin InSe photodetectors, Mater. Horiz. 7 (1) (2020) 252–262.
[98] J. Xu, T. Liu, H. Hu, Y. Zhai, K. Chen, N. Chen, X. Zhang, Design and optimization of tunneling photodetectors based on graphene/Al2O3/silicon heterostructures, Nanophotonics 9 (12) (2020) 3841–3848.
[99] O. Surucu, D.E. Yıldız, M. Yıldırım, A study on the dark and illuminated operation of Al/Si3N4/p-Si Schottky photodiodes: optoelectronic insights, Appl. Phys. A 130 (2) (2024) 103.
[100] D.E. Yıldız, A. Kocyigit, M. Yıldırım, Comparison of Al/TiO2/p-Si and Al/ZnO/p-Si photodetectors, Opt. Mater. 145 (2023) 114371.
[101] D.E. Yıldız, A. Karabulut, M. Yıldırım, N.A. Morley, R. Sahingoz, Photoelectrical performances of semiconductor-based devices having CoFe and CoFeNi magnetic interlayers, Phys. Scr. 99 (6) (2024) 065051.
[102] K. Czuba, Ł. Ciura, I. Sankowska, E. Papis-Polakowska, A. Jasik, The role of noise in specific detectivity of InAs/GaSb superlattice MWIR bariodes, Sensors 21 (21) (2021) 7005.
[103] J.H. Vella, L. Huang, N. Eedugurala, K.S. Mayer, T.N. Ng, J.D. Azoulay, Broadband infrared photodetection using a narrow bandgap conjugated polymer, Sci. Adv. 7 (24) (2021) eabg2418.
[104] F. Haenschke, E. Kessler, U. Dillner, A. Ihring, U. Schinkel, H.G. Meyer, New High Detectivity Linear Array for Analytical Measurement in the Room Temperature Range, in: Infrared Technology and Applications XXXVIII, 8353, SPIE, 2012, May, pp. 543–548.
[105] A. Caillas, P. Guyot-Sionnest, Uncooled high detectivity mid-infrared photoconductor using hgte quantum dots and nanoantennas, ACS Nano 18 (12) (2024) 8952–8960.
[106] K. Yılmaz, A. Akgoz, M. Cabuk, H. Karaagac, Karabulut, M. Yavuz, Electrical transport, optical and thermal properties of polyaniline–pumice composites, Mater. Chem. Phys. 130 (2011) 956–961.
[107] M.M.D. Ramos, H.M.G. Correia, Effects of electric field and charge distribution on nanoelectronic processes involving conducting polymers, Mater. Sci. Eng. C 26 (2006) 1002.
[108] N.D. Sankir, M. Sankir, M. Parlak, E lectrical properties and photoconductivity of polyaniline/sulfonated poly(arylene ether sulfone) composite films, Appl. Phys. A 95 (2009) 589–594.
[109] A. Kocyigit, D.E. Yıldız, N. Tasaltın, M. Yıldırım, Role of interfacial layer as PANI–silicene in Si-based photodiodes, J. Mater. Sci. 59 (2024) 9437–9454.
[110] N. Sunel, A.G. Sedef, M. Parlak, L. Toppare, Electronic properties of polyamide–PPy/metal junction and electrical conductivity of a typical sample at low temperatures, Mater. Chem. Phys. 91 (1) (2005) 227–232.
[111] V. Saxena, B.D. Malhotra, Prospects of conducting polymers in molecular electronics, Curr. Appl. Phys. 3 (2003) 293–305.
[112] R. Cabala, V. Meister, K. Potje-Kamloth, Effect of competitive doping on sensing properties of polypyrrole, J. Chem. Soc. Faraday Trans. 93 (1997) 131–137.
[113] A.F. Diaz, J.I. Castillo, A polymer electrode with variable conductivity: polypyrrole, J. Chem. Soc. Chem. Commun. 0 (1980) 397–398.
[114] P. Novák, K. Müller, K.S.V. Santhanam, O. Haas, Electrochemically active polymers for rechargeable batteries, Chem. Rev. 97 (1997) 207–282.
[115] H. Apaydin, D.E. Yildiz, A. Cirpan, L. Toppare, Optimizing the organic solar cell efficiency: role of the active layer thickness, Sol. Energy Mater. Sol. Cells 113 (2013) 100–105.

Abdulkerim Karabulut was born in Tekman/Erzurum/Turkey in 1986. He received his B.Sc. and Ph.D. degrees in physics from Ataturk University, Erzurum, Turkey, in 2010 and 2014, respectively. He works as a full-time Professor at Erzurum Technical University, Faculty of Science. His current research interests include especially the fabrication of MOS and MIS structures, semiconductor-based materials and photovoltaic applications. Abdulkerim Karabulut, who has numerous published articles, has an h-index of 25 and an i10-index of 46 based on citations to his published works. He is married and the father of Yahya Kerim.

Dilber Esra YILDIZ completed her undergraduate education at Gazi University in 2000 and her MSc and PhD at the same university in 2008. She is currently working as a Professor at Hitit University, Faculty of Science, Department of Physics. Her main research interests are Solid State and Materials Chemistry, Semiconductors and Optoelectronics. Dr. Dilber Esra Yıldız has a total of 107 publications, with a resulting h-index of 27 and an i10-index of 56 from citations to these works.

Murat YILDIRIM is a full-time professor at Selcuk University, Faculty of Science in Konya, Turkey. After receiving his BS degree in Physics Engineering from Hacettepe University, Faculty of Engineering in 1998, he received his MS and PhD degrees from Selcuk University in 2002 and 2010, respectively. His current research interests include synthesis of nanomaterials, composites, organic and hybrid structures and their application in device fabrication. He is the author or co-author of more than 150 scientific articles in international journals and conferences and four book chapters.